

RESEARCH ARTICLE | JANUARY 10 2022

# Instrumentation development and testing of a wind turbine blade for sub-scale wake studies FREE

Special Collection: [Wind Tunnel Research, Dynamics, and Scaling for Wind Energy](#)

A. Hassanzadeh ; J. Naughton  ; J. LoTufo; H. Hangan

 Check for updates

*Journal of Renewable and Sustainable Energy* 14, 013302 (2022)

<https://doi.org/10.1063/5.0042011>

 CHORUS

  
View  
Online

  
Export  
Citation

 CrossMark

## Articles You May Be Interested In

Aerodynamic study of a small wind turbine with emphasis on laminar and transition flows

*AIP Conference Proceedings* (June 2016)

Design of horizontal-axis wind turbine using blade element momentum method

*AIP Conference Proceedings* (October 2013)

Aerodynamic study of a stall regulated horizontal-axis wind turbine

*AIP Conference Proceedings* (October 2013)

**APL Energy**

**First Articles Online!**

**Read Now**

# Instrumentation development and testing of a wind turbine blade for sub-scale wake studies

Cite as: J. Renewable Sustainable Energy **14**, 013302 (2022); doi: 10.1063/5.0042011

Submitted: 27 December 2020 · Accepted: 17 December 2021 ·

Published Online: 10 January 2022





View Online



Export Citation



CrossMark

A. Hassanzadeh,<sup>1</sup>  J. Naughton,<sup>1,a)</sup>  J. LoTufo,<sup>2</sup> and H. Hangan<sup>2</sup>

## AFFILIATIONS

<sup>1</sup>Wind Energy Research Center, University of Wyoming, Laramie, Wyoming 82071, USA

<sup>2</sup>WindEEE Research Institute, Western University, London, Ontario N6A 3K7, Canada

Note: This paper is part of the special issue on Wind Tunnel Research, Dynamics, and Scaling for Wind Energy.

<sup>a)</sup> Author to whom correspondence should be addressed: [naughton@uwyo.edu](mailto:naughton@uwyo.edu)

## ABSTRACT

Wind turbine blade aerodynamics and the resulting wake flow are complex, and wind tunnel testing of these flows can provide critical insight. The data from such tests are also valuable for validation of numerical models. For experiments using sub-scale turbines to be useful, the blade aerodynamics and wakes must exhibit the important features observed in utility-scale turbine flows. In this work, ~1 m blades designed to produce physics relevant to larger scale turbines were manufactured and affixed to an existing turbine. One of the blades was instrumented for blade surface pressure measurements. Time-dependent surface pressure measurements coupled with instantaneous measurements of the inflow with Cobra probes and the wake with particle image velocimetry allowed for characterization of the inflow, blade flow, and near wake. The results demonstrate that the instrumentation was effective in characterizing the blade loading and the flow field. For the one test case discussed in this paper, the measurements of inflow, blade loading, and wake properties facilitate understanding of the wake's behavior.

Published under an exclusive license by AIP Publishing. <https://doi.org/10.1063/5.0042011>

## I. INTRODUCTION

Optimizing the design and operation of wind plants requires understanding of the complex interaction between the wind inflow and the wind turbines. In sub-scale studies, matching dimensionless parameters between the full-scale and sub-scale wind turbine blades to the degree possible ensures that the important physics are present. In response to this need, approaches have been developed to design blades specifically for sub-scale wake studies.<sup>1–5</sup> One of these blade design approaches<sup>2</sup> matches the non-dimensional sub-scale and full-scale force distributions to produce blade aerodynamics and the resulting sub-scale wake that exhibit features similar to those of the full-scale turbine. There have been a number of sub-scale experiments focused only on the wake,<sup>6–9</sup> but, to the authors' knowledge, no 2-m scale wind turbine test has included blade pressure measurements to characterize the blade aerodynamics. Since the wake arises from the interaction of the inflow with the blade, a full characterization of the wake requires both blade load and wake measurements.

The objective of this work is to develop instrumentation suitable for characterizing the inflow, blade load distribution, and wake of a 2-m diameter wind turbine containing important flow features associated with full-scale wind turbines. Three carbon-fiber blades were

manufactured of which one was equipped with pressure taps. A compact pressure system that fits within the turbine's hub was developed to measure the pressures from these taps. The blades were mounted to a turbine, and the system was demonstrated under controlled test conditions in the Wind Engineering, Energy and Environment (WindEEE) dome. Inflow and wake measurements were also carried out using Cobra probes and a Particle Image Velocimetry (PIV) system, respectively. The time-dependent inflow, blade pressures, and wake measurements indicate that the blade loading and the resulting wake can be effectively characterized. Furthermore, the blade loading measurements facilitate understanding of the wake's behavior.

## II. BACKGROUND

Experimental wind turbine wake studies have been carried out both in the field and in wind tunnels. Since they inherently capture all the important physics associated with wake development and evolution, field measurements are critical for the understanding of these flows.<sup>10,11</sup> However, the challenges associated with field measurements often make it hard to use the field data alone for validating computational models. For example, Bingol *et al.*<sup>12</sup> and Trujillo *et al.*<sup>13</sup> used Light Detection and Ranging (LiDAR) to study the instantaneous

velocity deficit behind a turbine. The span-wise position of the wake was studied and compared to different models. Only data from non-rainy days and with wind directions within  $\pm 15^\circ$  relative a meteorological mast direction were used. This example underscores the difficulty of making field measurements and their use for validation because selection of specific data and averaging of the boundary conditions are required. It should be noted that very long field campaigns are necessary to gather sufficient data to determine the statistical quantities necessary to provide meaningful insight into the wake, which adds additional complexity and cost.

In contrast, wind tunnel investigations present several advantages compared to field tests including controlled test conditions and the opportunity for detailed measurements. Several measurement techniques including surface pressure measurements for blade loading and Particle Image Velocimetry (PIV) and hot-wire anemometry for wake velocities have been employed in wind tunnel tests. A very limited number of large-scale wind tunnel experiments have been conducted.<sup>14,15</sup> The focus of these experiments was blade load distribution and flow-field measurements on wind turbines that were designed for maximum power efficiency. There have been a number of wakes from wind turbines with rotor diameters between 0.5 and 2.5 m that have been studied, but they did not perform blade load distribution measurements. For example, Hashemi Tari *et al.*<sup>7</sup> used PIV to investigate the flow dynamics in the near-wake of a 2.2-m diameter turbine designed for maximum power efficiency. There have also been a number of smaller wind turbines with rotor diameters less than 0.5 m used for wake studies. For instance, Khan *et al.*<sup>16</sup> performed PIV measurements in the wake of a geometrically scaled wind turbine to study the effects of two different inlet conditions on the wake.

Much has been learned about wind turbine wakes from these and other experimental studies. However, the shortcomings discussed above, missing physics and incomplete data sets, limit their usefulness. Thus, investigation of a sub-scale wind turbine that produces a wake similar to that of a full-scale turbine and of a size that makes instrumentation of the blades possible is needed. Measurements of the inflow, blade loading, and wake from such a turbine would deepen our understanding of wake development and evolution and provide data for improving and validating computational models. The present study was specifically developed to address this need.

### III. EXPERIMENTAL APPROACH

An overview of the experimental facility and blade fabrication is provided along with a description of the instrumentation used to make blade load and wake measurements.

#### A. Facility—WindEEE

Testing of the instrumented blade mounted on the sub-scale wind turbine was conducted in the Wind Engineering, Energy and Environment (WindEEE) dome, which has a hexagonal test chamber measuring 25 m across. A general description of the facility is provided by Hangan.<sup>17</sup> The facility is capable of different types of atmospheric flows, but a straight flow with uniform and shear profiles was used in this work. For the straight flow configuration, 60 fans along one wall of the hexagon configured in four rows of 15 fans each were in operation. Each of these fans is 0.8 m in diameter, and the fans produce a flow with a velocity of  $\sim 25$  m/s at a nominal power of 30 kW. The effective size of the tunnel is  $25 \times 14 \times 3.5$  m, and the tunnel is capable

of operating up to 30 m/s. For this study, the tunnel was operated at 7 m/s to achieve a tip speed ratio (TSR) of 9 at a reasonable turbine rotational rate of  $\sim 600$  rpm.

#### B. Wind turbine design and fabrication

A three-bladed wind turbine with a rotor diameter of 2 m was used to conduct the experiments. The blade design was performed using an inverse blade element momentum (BEM) method with the goal of producing wakes in the wind tunnel comparable to those of an industrial-scale wind turbine.<sup>2,18</sup> Two S-series airfoils, the S814<sup>19</sup> and S825,<sup>20</sup> were used to design the blade. The S814 is a 24% thick airfoil that was employed in the blade root region ( $r/R = 0.27$ ) to allow high structural strength, whereas the S825 is 17% thick and was used in the blade tip section ( $r/R \geq 0.53$ ). For  $0.27 < r/R < 0.53$ , the blade geometry smoothly transitioned from the S814 to the S825 profile. The tripped high-Re airfoils were employed in an attempt to achieve a comparable aerodynamic behavior for full-scale and sub-scale blades at both on-design and off-design conditions.<sup>21</sup> Figure 1 shows the chord, twist, and thickness-to-chord ratio ( $t/c$ ) distributions along the sub-scale turbine blade. The chord and twist angle start at their maximum values at the root section and decrease moving toward the blade tip region, which is consistent with a commercial wind turbine blade's geometry. It should be mentioned that the thickness-to-chord ratio was selected to be similar to that of the full-scale blade.<sup>1</sup> The three-dimensional rendering of the blade in Fig. 2 shows that the blade is different in appearance than a typical small wind turbine blade due to the relatively large chord in the root and small chord in the tip region.

A laminate schedule design was performed for the wind turbine blade using a finite element method (FEM). Optimal fiber orientations and laminate thicknesses were identified for maximum tip deflection of  $\sim 5$  mm or  $\sim 0.5\%$  of the blade length. The blade's stiffness is an important factor for the initial experiment, which is intended to demonstrate the potential of using the data for model validation. The simulation of highly deflected blades would need structural models to be coupled with CFD simulations, which makes the simulations more complicated. Another important criterion was the blade weight, which was required to be less than 0.5 kg. The sub-scale turbine was designed to rotate at a relatively high rotational speed ( $\sim 770$  RPM) to achieve a

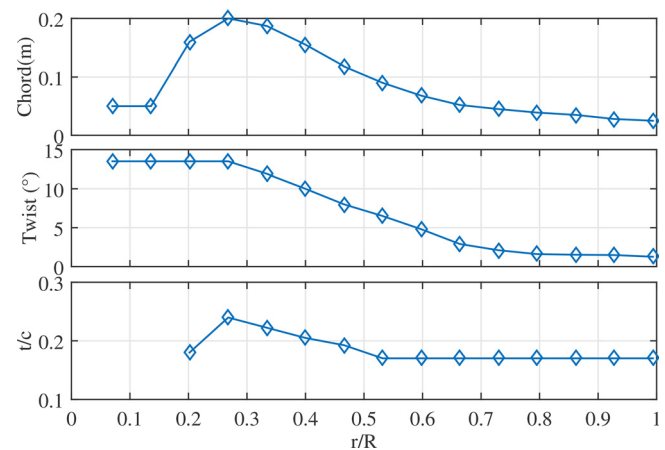


FIG. 1. Chord, twist angle, and thickness-to-chord ratio distributions along the blade.

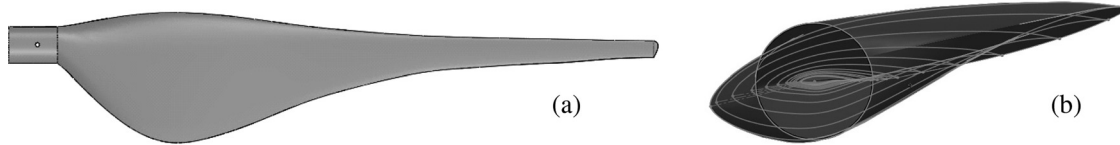


FIG. 2. Solid model of the sub-scale blade: (a) top view and (b) view along the axis of the blade.

reasonable chord Reynolds number  $Re_c \sim 200\,000$ ). Therefore, light blades were necessary to limit the inertial and centrifugal forces. To achieve weight and strength requirements, six plies of carbon fibers were aligned along the blade length or span, and two plies were aligned with the local chord for increasing bending stiffness. In addition, two plies were applied at a  $45^\circ$  angle to both chord and span to increase the torsional stiffness of the blade. More details regarding the FEM simulation results are given by Hassanzadeh.<sup>22</sup>

Based on the blade design and laminate schedule, three blades were manufactured by BE-Technologies, Ltd. Molds were CNC machined from 6061-T6 aluminum for both the pressure and suction sides of the blade as shown in Fig. 3(a). The layup of carbon plies was performed to achieve the required thickness. Once completed using a hand lay-up process, typical composite layup materials including bagging film, breather cloth, and gum tape were used, and the carbon plies were sealed around periphery of tool to ensure vacuum bag integrity. Each half of the blade was oven-cured under vacuum at the required temperature and pressure. Upon completion of this process, each half was precision machined to ensure proper alignment. After instrumenting one of the blades with pressure ports, weights were added to the two other blades to balance them. The two halves (pressure and suction sides) were then bonded together as shown in Fig. 3(b).

After blade fabrication, the actual geometry was measured at several span-wise locations using a contour gauge, and the results were verified by a Romer Arm measuring system. Figure 4 shows the original and the measured airfoil geometries. It can be observed that there is a shift in the geometry, particularly near the trailing edge (TE) of the blade sections. This occurs because the S814 and S825 airfoils were designed to have a sharp trailing edge, but the manufactured blades

required finite trailing-edge thickness. Even though the TE thickness is  $\sim 3.3$  mm all along the blade, the impact on the geometry is most noticeable near the blade tip since the chord and thickness of the blade in the tip section are smaller than those in the root section. It should be mentioned that the actual blade geometry was used for all subsequent calculations that require it.

One of the blades was equipped with pressure taps to acquire detailed surface pressure data to provide distributed load information. 126 pressure ports with a diameter of 0.86 mm at 6 different span-wise stations ( $r/R = 0.20, 0.27, 0.40, 0.53, 0.73,$  and  $0.86$ ) were drilled on the pressure and suction sides of the blade. Figure 4 shows the location of the pressure ports at selected span-wise stations. Fewer pressure ports were placed in the blade tip region than the root region as the physical chord length was smaller. Pressure taps were more densely distributed near the blade leading edge (LE) to better resolve the pronounced pressure gradients typically present in that region. The interior of the suction side of the instrumented blade is shown in Fig. 5 that shows the 3D printed ribs that were placed and secured inside the blade's shell for easy and secure connection of the pressure taps to vinyl tubing. The vinyl tubes were connected to pressure scanners during the experiment.

Since the operating wind tunnel testing conditions yield chord Reynolds numbers that can lead to laminar or transitional boundary layer state on the blade, boundary layer trip strips with thickness and extent of approximately 0.2–1 mm (depend on the local chord length) were applied. The trip was applied at  $\sim 5\%$  of the chord from the leading edge on both top and bottom surfaces. The trip helps to promote transition to turbulent flow. This tripping approach was taken to yield airfoil section performance similar to that obtained at higher Reynolds



FIG. 3. Blade fabrication details: (a) aluminum molds with the resulting blade surfaces and (b) bonding of the blade surfaces.

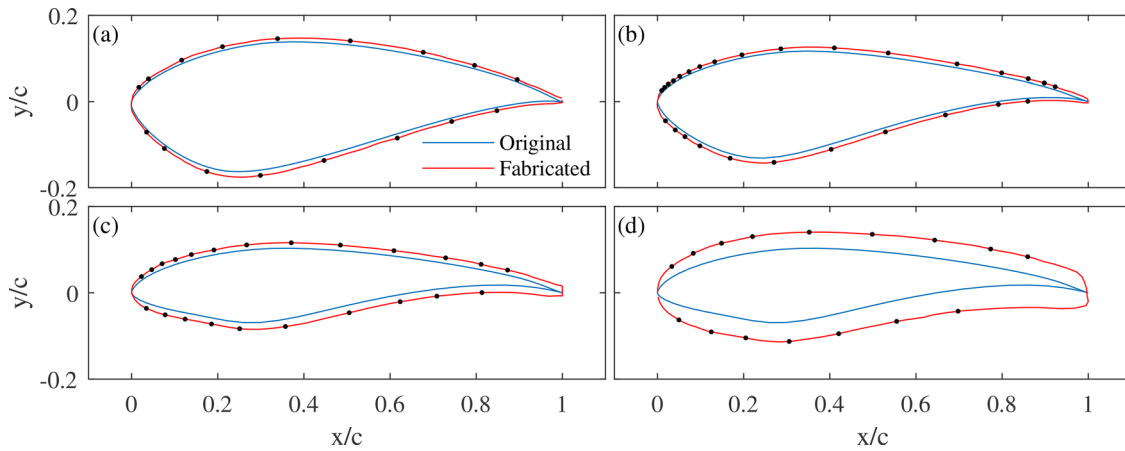


FIG. 4. Comparison of the specified and measured airfoil geometry with pressure port locations shown as black dots at several span-wise locations: (a)  $r/R = 0.20$ , (b)  $r/R = 0.27$ , (c)  $r/R = 0.53$ , and (d)  $r/R = 0.86$ .

numbers. Gasket sealant was used to apply fine grit sand particles to the blade surface.

The three blades were mounted to a custom hub that was designed to assure the secure connection of the blades and a pressure measurement system to the turbine. Two holes on the root section of each blade were drilled for a blade pitch angle of zero, and the blades were locked to the hub with two 1/4–20 stainless steel screws. The hub was then mounted to an existing turbine model with a hub height of 1.5 m. The turbine model allowed for accurate control of the tip speed ratio.

### C. Instrumentation

To carry out blade load and flow field measurements on the 2 m diameter wind turbine, specialized instrumentation was required. A schematic of the experimental setup in the WindEEE dome for these measurements is shown in Fig. 6, where the Cartesian coordinate system is defined.

#### 1. Cobra probe

A vertical array of five Cobra probes at upstream of the turbine ( $x/D = -1.1$ ,  $y/D = -0.7$ ) was used to measure the inflow velocity (see Fig. 6). The Cobra Probe is a multi-hole pressure probe that resolves three components of velocity and local static pressure. The probes were placed at  $y/D = -0.7$  to avoid introducing artifacts in the  $y/D = 0$  plane where the wake was measured. The Cobra probes were continuously sampled throughout a test at high frequency, and the sampled data were decimated to a rate of 1250 Hz by low-pass filtering and down-sampling. The probes are quoted to have response out to 2000 Hz according to the manufacturer.<sup>23</sup> The frequency content



FIG. 5. Blade interior with surface pressure taps and tubing.

of the inflow is limited to several hundred hertz, so the response of the probes was considered sufficient. A typical run time for each test case was 8 min, which is linked to the measurement uncertainty requirements of the blade surface pressures. The mean velocities, turbulence intensities, and flow angles (yaw and pitch angles) were computed from instantaneous velocities. The yaw angle is the angle between the local velocity direction in the  $x - y$  plane and the  $x$ -axis (rotation angle about the  $z$ -axis), and the pitch is the angle between the local velocity vector and the  $x - y$  plane. The collected samples during each test case were used to calculate the mean velocities, and random error with the 95% confidence interval is approximately 0.2% and 1.1% for the uniform and shear inflow cases, respectively. The systematic uncertainty of the cobra probes depends on turbulence levels, but is generally within 0.5 m/s up to about 30% turbulence intensity according to the manufacturer.<sup>23</sup> Considering the 7 m/s average wind velocity in the experiments, the systematic uncertainty of the probes is about 7%. More details regarding Cobra probe data analysis are discussed by Hassanzadeh.<sup>24</sup>

#### 2. Pressure system

A compact pressure system that fit within the turbine’s hub was designed specifically for this study. The system’s hardware and

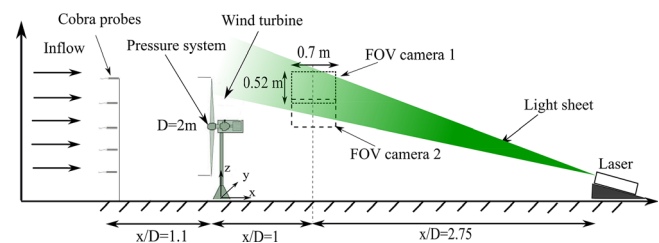


FIG. 6. Schematic of the experimental setup in the WindEEE dome for blade load measurements and PIV measurements at  $x/D = 1$ . Hassanzadeh *et al.*, “Aerodynamic load distribution and wake measurements on a sub-scale wind turbine,” *J. Phys.: Conf. Ser.* **1452**, 012059 (2019). Copyright 2019 Authors, licensed under a Creative Commons Attribution (CC BY 3.0) license.

software subsystems are described, and a brief discussion of data analysis is presented.

Pressure measurements on a rotating wind turbine are challenging. Pressure transducers are sensitive to external forces, and, as a result, the effects of centrifugal force on rotating pressure transducers need to be considered. Additionally, there are some difficulties of routing the pressure signal, power, and communications from the rotating blade to the tower. To address those challenges, a stand-alone, hub-mounted pressure measurement system was developed. Figure 7(a) shows a schematic of the hardware and software subsystems for the pressure system. As shown in Fig. 7(b), the packaged pressure system was integrated into a chassis that fit within the custom hub described above.

The hardware components required to perform the blade pressure distribution measurements are shown in Fig. 7. This system was derived from that previously used for measurements on two-dimensional airfoils.<sup>25</sup> This design specifically addresses the challenges particular to a small wind turbine.

Unsteady pressure data were acquired through the use of two Electronic Pressure Scanners (ESPs) that were connected to the pressure ports on the instrumented blade using vinyl tubing. The ESPs used in this study can scan 32 pressure ports. A custom-built printed circuit board (PCB) was used to provide an interface between the transducer and the data acquisition system and to amplify the pressure transducer signal. Control of the ESP modules was carried out by a National Instruments MyRIO equipped with a field programmable gate array (FPGA). Sampling at 20 kHz over 32 channels for each module led to a sampling rate of 625 Hz per channel. The pressure data were recorded for 8 min ensuring a pressure coefficient precision uncertainty of 0.05. To account for variations in testing conditions (tunnel pressure and temperature), the pressure transducers were calibrated daily using a 6-point linear fit. As pressure in the rotor plane is different than atmospheric pressure, the reference pressure port of the transducers was connected to a closed basket in the hub. For any variation of the temperature inside the turbine's hub during the experiment, the temperature was recorded using a digital temperature sensor at a rate of 1 Hz. The temperature variation inside the pressure system is important as it can affect the reference pressure used for the transducer.

The blade position is needed to associate the pressure measurements with the corresponding blade location. For blade position and rotational speed measurements, a proximity sensor was mounted on the turbine's hub to record the blade passage. The proximity sensor was sampled at a frequency of 20 kHz.

The power for the entire system was provided by a 6800 mAh lithium battery that provided sufficient energy to the system such that it could operate for more than 5 h. The data collected during testing were recorded in text format and were stored in a 32 GB Universal Serial Bus (USB) flash drive. The typical amount of data stored in an 8-min run was about 200 MB.

Data acquisition of the signals from the hardware was controlled using an in-house LabVIEW program. In order to address the challenges of communicating between the rotating blade and the tower, communication between the host computer and the real-time processor (RT) was accomplished using WiFi, as shown in Fig. 7(a). WiFi communication was used for setting operating parameters as well as transmitting some data during the experiment to monitor the system's state and to verify that the system was operational. The communication between the FPGA and RT processor used a first-in first-out (FIFO) buffer [see Fig. 7(a)]. One FIFO transferred data from the FPGA to the RT (to flow the data from sensors to the USB flash drive), and a second FIFO transferred the operating parameters from the RT to the FPGA.

Certain physical phenomena manifest themselves on the actual pressure data and must be accounted for when conducting pressure measurements on a wind turbine blade. In the current setup, the pressure measurements were conducted remotely, where the ESPs were connected to the surface ports through large length-to-diameter pressure tubing (with length-to-diameter ratios up to 1100). In such a configuration, the tubing affected the pressure measurements by attenuating the signal and introducing a time lag as compared to the original signal. These effects in the pressure signals were corrected using a Weiner filtered system response model (WFSRM) that depends on tubing geometry and atmospheric conditions.<sup>26</sup> To fine tune the WFSRM model, a known signal was applied to each tap. Both the input pressure pulse at the tap and the pressure at the corresponding ESP channel were measured simultaneously. Comparing the

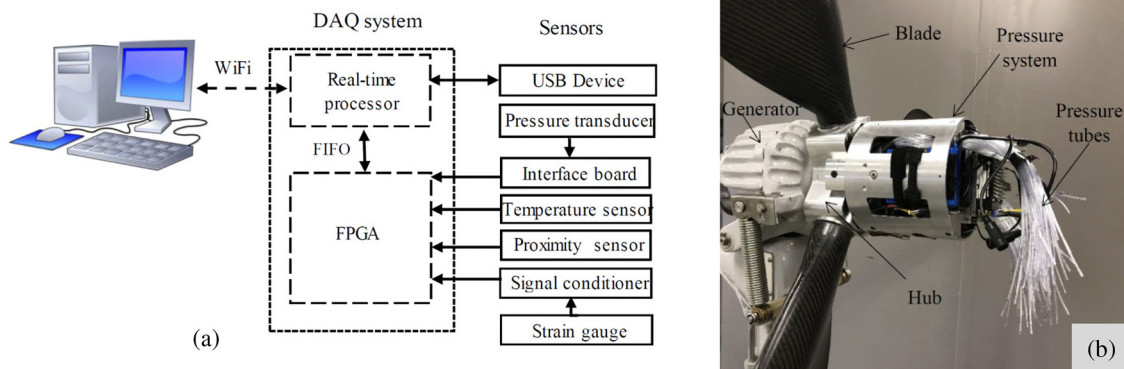


**FIG. 7.** Pressure measurement system: (a) schematic of the hardware and software subsystems and (b) the pressure system mounted to the turbine's hub for blade surface pressure measurements. Tubes have not been connected to the Electronic Pressure Scanners (ESPs), and the nose cone is removed. Hassanzadeh *et al.*, "Aerodynamic load distribution and wake measurements on a sub-scale wind turbine," *J. Phys.: Conf. Ser.* **1452**, 012059 (2019). Copyright 2019 Authors, licensed under a Creative Commons Attribution (CC BY 3.0) license.

measured and WFSRM reconstructed signals allowed for the modeled tubing geometry to be slightly modified to produce an optimal reconstruction. Repeating this process for each tap on the blade allowed the correction of the pressure signals from each tap. The results of this process indicated that the pressures could be corrected accurately to  $\sim 600$  Hz, with frequencies greater than that attenuated. Based on the turbine's rotational speed (about 10 rev/s) and the frequency response of the correction, it was concluded that the blade pressure data were resolved with a temporal uncertainty that represents a delay of  $6^\circ$  of rotation. For additional details on the details of the WFSRM and its application, see Hind *et al.*<sup>27</sup> and Nikoueeyan *et al.*<sup>28</sup> Another important phenomenon to measuring pressure in rotating reference frames is the centrifugal force effect, which occurs because the column of air trapped between the sensor and the port exerts a net negative force on the sensor diaphragm as the blade rotates.<sup>29</sup> The resulting difference in measured and actual surface pressure, due to the centrifugal force, is a function of span-wise location of the port and the blade rotation rate,

$$P_{cen} = 0.5\rho r_{sec}^2\omega^2, \quad (1)$$

where  $\rho$ ,  $r_{sec}$ , and  $\omega$  are the density, the port's span-wise location from the center of rotation, and the turbine rotation rate, respectively.

After correction, azimuthal averaging of the pressure data were performed. For each port, every pressure data point was binned based on its azimuthal angle, and the pressure data in every bin were averaged. The azimuthal-averaged pressure for each port was calculated from 1000 continual pressure records of 200 samples during 8 min of testing. These data were separated into 360 phase bins, resulting in approximately 550 samples per bin. From the resulting pressure distributions, aerodynamic properties of the airfoil were calculated. The normal and tangential forces were obtained by integrating the azimuthal-averaged pressures at each blade span over the suction and pressure surfaces.

The uncertainty of the pressure measurements has been determined, and the details are provided in Refs. 22 and 24. Pressure coefficients at a specific azimuthal angle are presented with their corresponding uncertainties in Fig. 8. The uncertainty values are higher for the shear inflow case compared to those of the uniform inflow at two different span-wise stations ( $r/R = 0.27$ , and  $r/R = 0.73$ ) due to the higher turbulence intensity in the shear inflow. Relatively constant uncertainty can be seen along the local chord length for both cases as the flow is attached on the airfoils. More variation in uncertainty would be expected if the flow separated. In order to calculate the

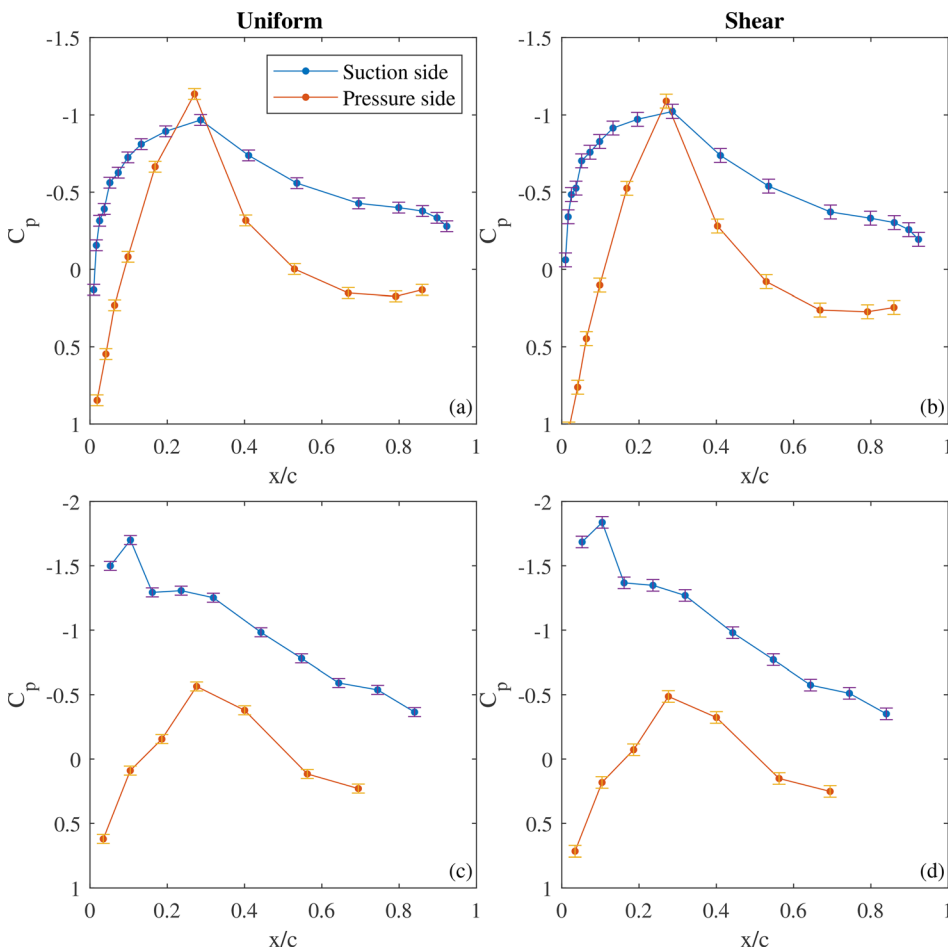


FIG. 8. Pressure coefficient and corresponding uncertainties for the uniform and shear inflow cases at  $\psi = 0^\circ$ : (a) and (b)  $r/R = 0.27$  and (c) and (d)  $r/R = 0.73$ .

uncertainty of the blade normal and tangential forces, the pressure uncertainty was propagated through the integral (summation for the discrete data) used to calculate the loads. The details of the uncertainty propagation can be found in Ref. 22. Figure 9 shows the uncertainty of the two different inflow cases at a tip speed ratio of 9. As expected, the uncertainties of both normal and tangential forces are higher for the shear inflow case than those of the uniform inflow case. These results are typical of the uncertainties determined for the cases studied here.

### 3. Particle image velocimetry (PIV)

A PIV system was employed to measure two components of velocity behind the turbine in a vertical plane between the hub and the blade tip at two different locations. The PIV data were collected primarily to capture mean wake velocities to better understand the interaction of the inflow with the blade and the resulting wake produced. As this was an initial attempt at obtaining PIV measurements in this wake and the conditions were challenging, no further analysis beyond the mean and wake was attempted. Figure 6 shows the PIV set-up for near-wake measurements at  $x/D = 1$ . A laser with an energy of 60 mJ/pulse at 0.1–1 kHz, a frequency-doubled wavelength of 527 nm, and a beam diameter of 3 mm was employed to illuminate the flow field. A cylindrical lens was positioned in front of the laser head to convert the beam into a two-dimensional sheet. The laser was positioned at  $x/D = 2.75$  from the center of the area of interest (either  $x/D = 1$  and  $x/D = 5$ ) pointing upward with an angle of  $27^\circ$  for both cases. As shown in Fig. 6, a portion of the area of interest (from the hub height to above the blade tip) was illuminated by the laser. Two 12-megapixel cameras (IO Industries Flare 12M125-CL), each with a 105 mm  $f/2D$  Nikon AF DC-NIKKOR lenses, were used to capture images. Considering an  $f$ -stop of 8, the diffraction spot size was calculated using the method presented by Adrian and Westerweel<sup>30</sup> and was found to be approximately  $11 \mu\text{m}$ . The cameras were positioned at  $y/D = -0.85$  at two different heights ( $z/D = 0.9$  and  $1.1$ ) to cover the areas of interest at  $x/D = 1$  and  $x/D = 5$ . A calibration plate was used to calibrate the cameras such that image space could be connected to physical space. The cameras were adjusted to cover the desired interrogation regions and then focused on the calibration plate such that particles would be captured within the laser sheets aligned to

pass along the calibration plate. The camera resolution was  $4096 \times 3072$  pixels, corresponding to an image physical space of 70 cm wide by 52 cm height. The overlap of the two camera's view was 10 cm in the image plane. The time interval between the light sheet pulses was chosen to be  $300 \mu\text{s}$  to ensure that the particles moved less than one quarter of the length of the initial interrogation region. Images were acquired via IO Industries Core view software as 8 bit grayscale images and were stored as Tagged Image File Format (TIFF) format. Due to limitation in the illumination and seeding, a significant number of images were needed to obtain converged mean and variance values. The PIV data were collected for 2 min per test case with a sampling frequency of 55 Hz, resulting in 6600 images. Three Ultratec CLF-4460 commercial fog generators were used to seed the test chamber with nontoxic, water-based particles with a diameter of 1–5  $\mu\text{m}$ .<sup>31</sup>

LaVision's DaVis software was used to process the raw images. Velocity data were calculated using a multi-pass, cross correlation method for each camera. A  $128 \times 128$  pixel initial interrogation region was used with an iteratively decreasing window size to a  $64 \times 64$  pixel interrogation region with a 50% overlap of the regions. This resulted in a nominal spatial resolution of roughly 5.4 mm for the velocity fields. Even though the simplest way to improve the spatial resolution is to reduce the interrogation window size, this is accomplished at the cost of increasing the uncertainty level.<sup>32,33</sup> 2000 images were averaged to calculate the mean velocities, and the random errors with the 95% confidence interval for the mean velocities at uniform and shear inflow cases are  $\sim 3.1\%$  and  $\sim 5.2\%$ , respectively. The systematic uncertainty of the PIV data is not considered in this work. Once velocity values were calculated from both cameras, the vector fields were merged to create one large region.

### D. Test cases

Using the instrumentation discussed above, a number of test cases were conducted using the 2-m diameter wind turbine. Since wind turbine blade aerodynamics and wakes are highly dependent on the inflow, the effects of uniform and shear inflow were considered. For the shear inflow, a series of spires with roughness elements (on the ground) were used upwind of the turbine to create a shear profile. The blade aerodynamics and wake are also affected by the turbine's operating condition. As a result, the turbine's rotational rate was varied such

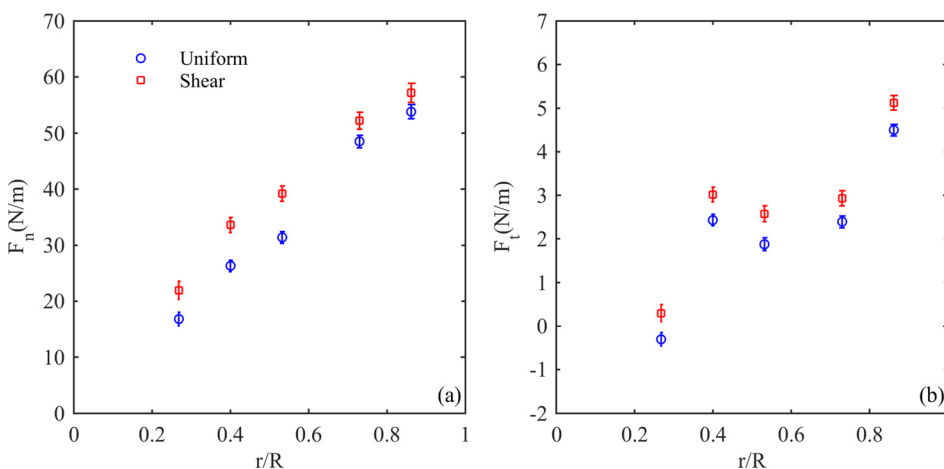


FIG. 9. Forces and corresponding uncertainties for the uniform and shear inflow cases for a TSR = 9 at  $\psi = 0^\circ$ : (a) normal force and (b) tangential force.

that tip-speed-ratio (TSR) of 9 (an on-design condition) and 5 (an off-design condition) could be examined. Multiple runs under the same conditions were necessary for some measurements. An example case (uniform inflow and a tip speed ratio of 9) is discussed here to demonstrate the typical results that were obtained using the hardware and instrumentation discussed. Further analysis of the results under different inflows and turbine operating conditions is presented in Ref. 24.

#### IV. RESULTS AND DISCUSSION

Measuring the properties of the inflow to the turbine is important to establish the conditions the turbine experiences. Therefore, the time-averaged axial velocity, turbulence intensity, and flow angles were acquired upstream of the turbine using Cobra probes (see Fig. 10). The mean velocity profiles are nearly constant as expected for the uniform inflow case. The turbulence intensities associated with the axial and vertical velocities ( $I_{uu}$  and  $I_{vv}$ , respectively) are nearly constant at about 7%, but the  $I_{vw}$  varies between 8% and 10%. The pitch angle is less than  $2^\circ$  for all measurements, but the yaw angle decreases with increasing height to  $-5^\circ$ . This is likely the result of the Cobra probes location in the induction zone where some outward flow is expected as the flow slows at the Cobra probes locations ( $x/D = -1.1$  and  $y/D = -0.7$  from the center of rotor).

In addition to characterizing the inflow, measurement of unsteady blade surface pressures is critical to characterizing the blade loading and resulting wake. Due to the large amount of spatial and temporal pressure data obtained on the rotating wind turbine blade, portraying the evolution of the pressure distribution over a complete blade revolution is challenging. To address this issue, azimuthally averaged pressure-coefficient contours are used. Figure 11 shows the pressure distributions for both suction and pressure surfaces of the S814 airfoil at the  $r/R = 0.27$  span-wise location for the uniform inflow and  $TSR = 9$  case. The  $x$ -axes show the  $x/c$  or relative chord location on the airfoil surface, and the azimuthal angle is represented on the  $y$ -axes. The color scale represents the magnitude of the pressure coefficient, with red showing the maximum pressure coefficient and blue showing the minimum, or maximum suction, pressure coefficient.

Note that the iso- $C_p$  lines are overlaid on the pressure distributions to help identify the changes in surface pressure. Conventional pressure coefficient plots at selected phases are shown in Fig. 11 by the dashed lines to aid the interpretation of the figure. It is evident that the flow is attached on both the pressure and suction surfaces throughout the blade rotation. Tower effects can be observed on the suction side in the region around  $\psi = 180^\circ$  where the peak suction pressure drops. Negative pressure coefficient values can be seen on the pressure side of the S814 airfoil, where the flow accelerates because of the high degree of curvature on the pressure side of this airfoil. These negative  $C_p$ -values occur on the pressure side of thick airfoils when the angle of attack is low. For more details regarding pressure data at different span-wise locations along the blade, see Hassanzadeh *et al.*<sup>24</sup> and Hassanzadeh.<sup>22</sup>

The azimuthally averaged pressures were used to calculate blade loading. The normal and tangential forces were calculated by integrating the azimuthally averaged pressures at each blade span over the suction and pressure surfaces. Having the blade load distribution allows for comparison of different load cases and between measured and simulated loads. Figure 12 compares the experimental data and blade element momentum (BEM) results. The results indicate that the normal force is higher in the blade outboard section compared to that of the inboard section. In addition, the blade outboard section has a greater contribution to the torque compared to the inboard section. It is also evident that BEM slightly underestimates the normal force, but slightly overestimates the tangential force compared to the experimental data. The calculated normal and tangential forces determined from the pressure data are used to compute the lift and drag coefficients using the inflow angles. Note that the inflow angles were not experimentally measured, and thus they were determined using BEM, which provides only an estimate of the true blade inflow angle. A summary of the lift and drag coefficients from experimental data and XFOIL is shown in Fig. 13. The actual airfoil shapes were used in the XFOIL analysis. It is shown that XFOIL slightly underestimates the lift and the pressure drag across the blade compared to the experimental data. The integrated normal and tangential forces across the blade were used to determine the power and thrust coefficients. These values are tabulated in Table I for the present blade loads measurements.

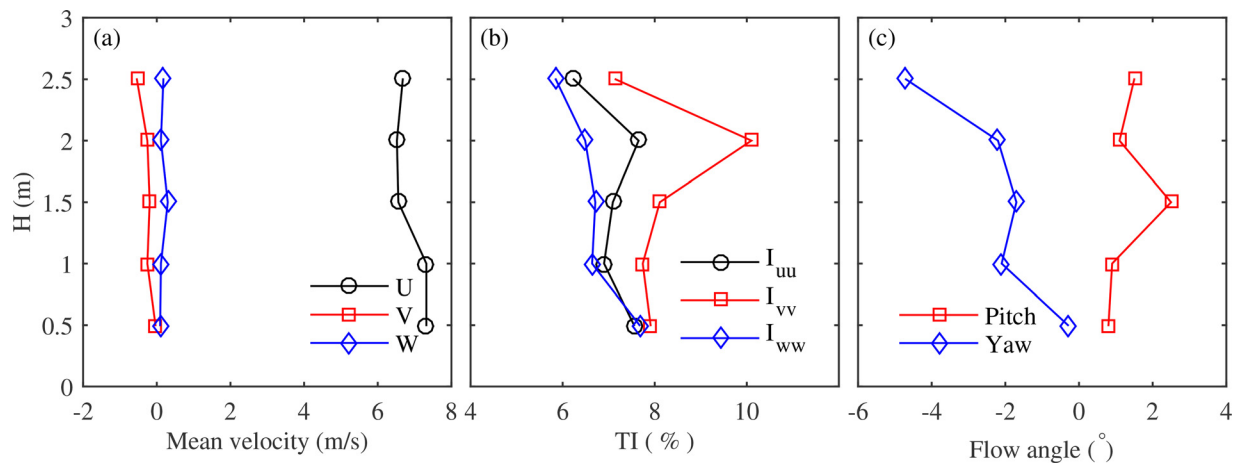


FIG. 10. Inflow characteristics: (a) mean velocity, (b) turbulence intensity (TI), and (c) flow angle profiles for the uniform inflow,  $TSR = 9$  case. For reference, the hub height of the turbine is 1.5 m.

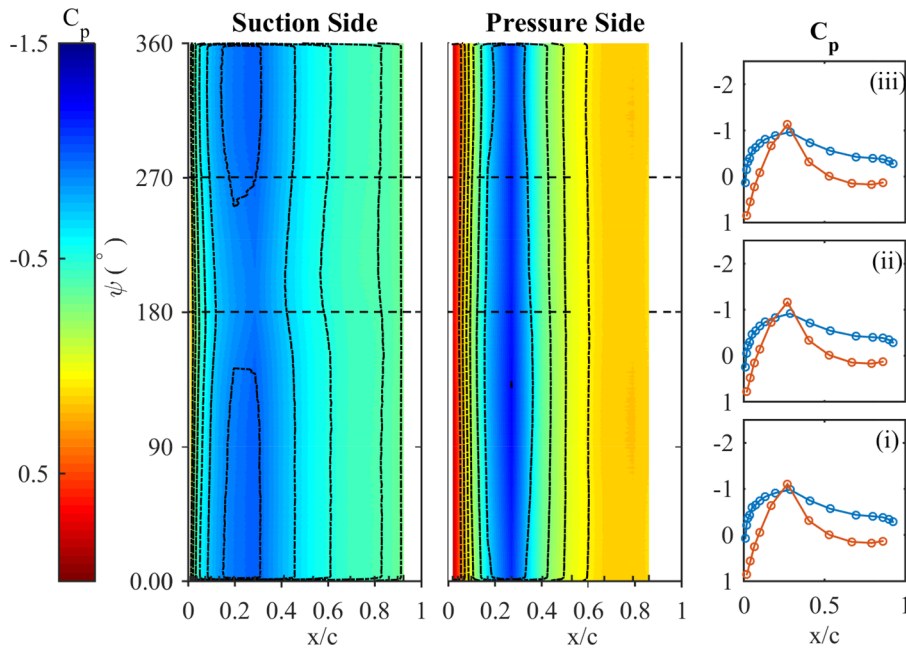


FIG. 11. Azimuthally averaged pressure distributions at different azimuthal angles for suction and pressure sides of the S814 airfoil at  $r/R = 0.27$ . Traditional pressure coefficient plots ( $\circ$ —pressure side and  $\circ$ —suction side) are shown for selected azimuths [(i)–(iii) correspond to  $\psi = 0^\circ$ ,  $180^\circ$ , and  $270^\circ$ , respectively] and are marked by the dashed lines for reference.

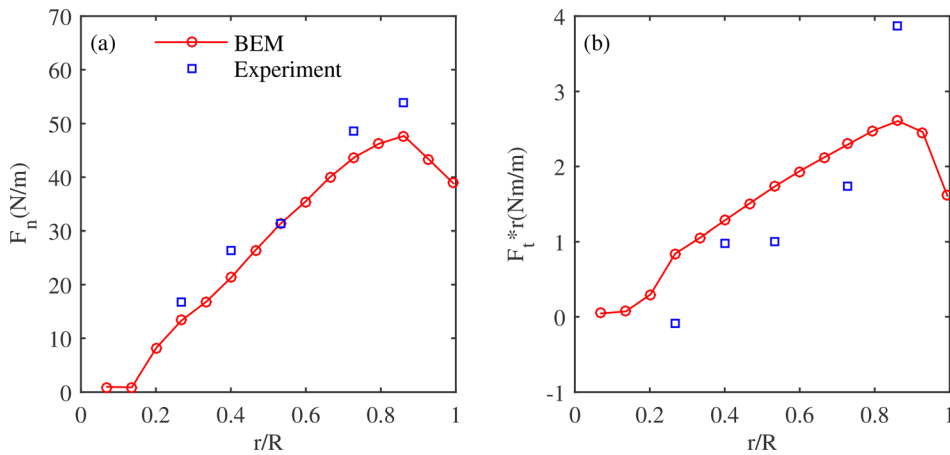


FIG. 12. Blade load distributions from the experiment and BEM model at  $\psi = 0^\circ$ : (a) normal force and (b) tangential force multiplied by radius.

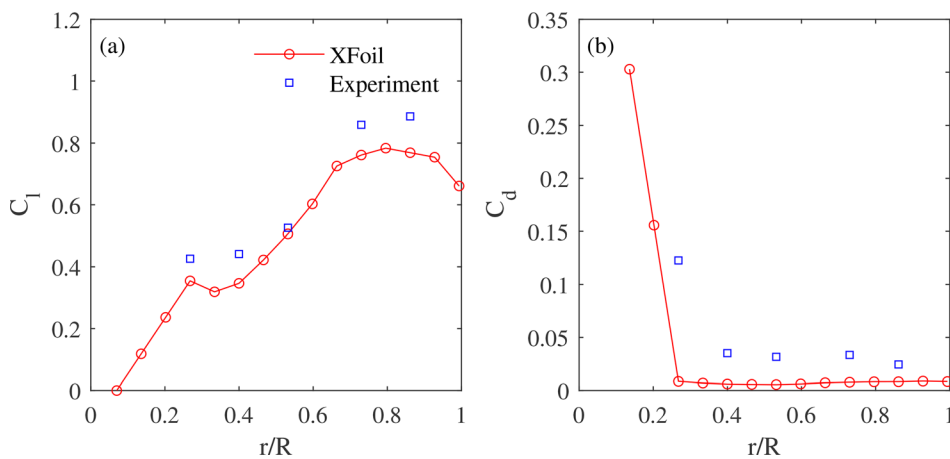


FIG. 13. Aerodynamics coefficients from the experiment and XFOIL at  $\psi = 0^\circ$ : (a) lift and (b) drag.

TABLE I. Power and thrust coefficients for the blade load measurements presented.

$U$ (m/s)	Rotational speed (RPM)	Power coefficient	Thrust coefficient
6.8	605	0.45	0.89

The velocity distributions measured by PIV were used to characterize the wake behind the turbine. The PIV measurements were obtained in a vertical plane behind the turbine. Wake velocity and turbulence intensity profiles are shown in Fig. 14 at  $x/D = 1$  and  $x/D = 5$  along with the inflow values from Cobra probes. The velocity deficit is lower at the  $x/D = 5$  compared to that at  $x/D = 1$  because of the wake recovery. At  $x/D = 1$ , the turbulence intensity is highest near the blade tip ( $r/R = 1$ ) due to the presence of tip vortices. In addition, the TI level in the inboard section is similar to that of the inflow. Similar results were reported by Chamorro and Porté-Agel<sup>34</sup> and Tian *et al.*,<sup>35</sup> where wake flow measurements were conducted using a point-wise cross-wire and a PIV measurements, respectively. At  $x/D = 5$ , the turbulence intensity level is relatively uniform, and it is higher compared to the inflow due to the turbulence production and mixing in the wake linked to the recovery of the axial velocity deficit.

The blade load distributions were coupled with wake velocities to understand the flow behavior in the wake. As shown in Fig. 12(a), the normal force peaks at  $\sim r/R = 0.8$ , which results in more momentum extraction from the flow at this radius. Therefore, it would be expected that this radial region would have the highest velocity deficit in the near wake ( $x/D = 1$ ), which can be observed in Fig. 14(a). Thus, a clear link is observed between the normal force distribution on the blade and axial wake velocity deficit in the wake. A more detailed analysis of the blade load distributions and wake velocities and their relationships is presented by Hassanzadeh *et al.*<sup>24</sup>

V. CONCLUSIONS

Characterization of the inflow, blade loads, and near-wake flow has been demonstrated for 2-m diameter turbine with blades designed to produce physics relevant to larger scale turbines. A specifically

designed hub-mounted, stand-alone pressure measurement system was used to determine blade loading, and PIV was used to measure a portion of the near wake. The inflow, blade loading, and wake data were coupled for better understanding the wake behavior, and the results show a direct relationship between the measured blade loading and the observed wake structure.

The primary intent of this work was to demonstrate the value of coupled flow-field measurements and blade surface-pressure measurements. Critical to this effort was the measurement of unsteady pressure on a small wind-turbine blade using a compact instrumentation package. Although the unsteadiness was small for the conditions measured, it was effectively captured by the system. Such measurements will be critical in off-design conditions (such as high yaw cases) where the azimuthal dependence of the pressure distributions will be much more pronounced. Furthermore, the results indicate that the extra effort required to obtain inflow and distributed blade load measurements is justified in wake measurement campaigns. Such measurements facilitate the interpretation of the measured wake profiles, which is necessary for fully understanding wake development. For this reason, comparing modeled and experimental blade load data is necessary to wake modeling validation efforts.

It is anticipated that, having demonstrated the feasibility of these measurements in a small 2-m diameter wind turbine, similar tests in off-design conditions (high yaw, inflow gusts, etc) would benefit from unsteady blade loading measurements. Future measurements in this flow would benefit from the better understanding of the use of PIV in this flow-field gained in this experiment. Inflow, blade load and complete wake measurements will allow for a momentum balance analysis that will help to definitively understand the interaction of the inflow with the blade and the resulting development of the near wake. As wake control receives continued interest, the capability to better understand load modification and resulting wake movement would benefit from such measurements. The impact of a wake on a downstream turbine is another potential use of the methods developed here. Such a study would provide measurements of the unsteady blade loads experienced by the waked turbine, allowing for better understanding of power production and loading impacts of a waked inflow.

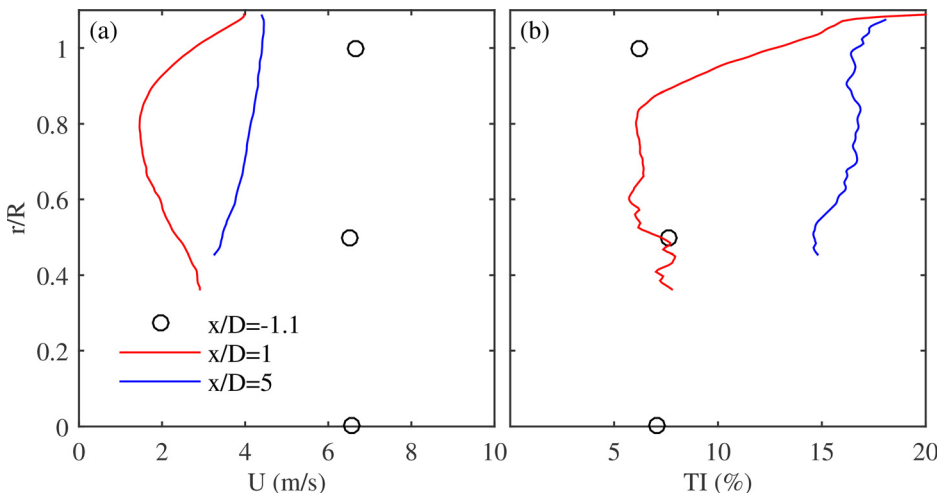


FIG. 14. Velocity profiles in the wake (lines) at two different downstream locations along with the inflow data (o): (a) axial mean velocity and (b) turbulence intensity.

## ACKNOWLEDGMENTS

This work was supported by the U.S. Department of Energy, Office of Science, Basic Energy Sciences, under Award No. DE-SC0012671. The authors would also like to acknowledge the contributions and comments from those who helped with this research: Faisal Bhuiyan and Ray Fertig for blade FEM simulations, Pourya Nikoueeyan for the pressure system, Lawrence D. Willey, Manjinder Singh, and Michael Hind for blade instrumentation, and Gerald Dafoe for assistance with testing.

## AUTHOR DECLARATIONS

## Conflict of Interest

The authors have no conflicts of interest to disclose.

## DATA AVAILABILITY

The data that support the findings of this study are available from the corresponding author upon reasonable request.

## REFERENCES

- <sup>1</sup>C. L. Kelley, "Aerodynamic design of the national rotor testbed," Report No. SAND2015-8985PE (Sandia National Laboratory, 2015).
- <sup>2</sup>A. Hassanzadeh, J. W. Naughton, C. L. Kelley, and D. C. Maniaci, "Wind turbine blade design for subscale testing," *J. Phys.: Conf. Ser.* **753**, 022048 (2016).
- <sup>3</sup>M. F. Howland, J. Bossuyt, L. A. Martínez-Tossas, J. Meyers, and C. Meneveau, "Wake structure in actuator disk models of wind turbines in yaw under uniform inflow conditions," *J. Renewable Sustainable Energy* **8**, 043301 (2016).
- <sup>4</sup>I. Bayati, M. Belloli, L. Bernini, and A. Zasso, "Aerodynamic design methodology for wind tunnel tests of wind turbine rotors," *J. Wind Eng. Ind. Aerodyn.* **167**, 217–227 (2017).
- <sup>5</sup>S. Cole, G. Hess, and M. Wosnik, "Design of a controllable one-meter scale research wind turbine," in *ASME 2017 Fluids Engineering Division Summer Meeting, Waikoloa, Hawaii, July 30–August 3 2017* (ASME, 2017).
- <sup>6</sup>L. Lignarolo, D. Ragni, C. Krishnaswami, Q. Chen, C. S. Ferreira, and G. Van Bussel, "Experimental analysis of the wake of a horizontal-axis wind-turbine model," *Renewable Energy* **70**, 31–46 (2014).
- <sup>7</sup>P. Hashemi Tari, K. Siddiqui, and H. Hangan, "Flow characterization in the near-wake region of a horizontal axis wind turbine," *Wind Energy* **19**, 1249–1267 (2016).
- <sup>8</sup>J. Schottler, A. Hölling, J. Peinke, and M. Hölling, "Design and implementation of a controllable model wind turbine for experimental studies," *J. Phys.: Conf. Ser.* **753**, 072030 (2016).
- <sup>9</sup>G. Campanardi, D. Grassi, A. Zanotti, E. M. Nanos, F. Campagnolo, A. Croce, and C. L. Bottasso, "Stereo particle image velocimetry set up for measurements in the wake of scaled wind turbines," *J. Phys.: Conf. Ser.* **882**, 012003 (2017).
- <sup>10</sup>M. L. Aitken, R. M. Banta, Y. L. Pichugina, and J. K. Lundquist, "Quantifying wind turbine wake characteristics from scanning remote sensor data," *J. Atmos. Oceanic Technol.* **31**, 765–787 (2014).
- <sup>11</sup>G. V. Iungo, Y.-T. Wu, and F. Porté-Agel, "Field measurements of wind turbine wakes with lidars," *J. Atmos. Oceanic Technol.* **30**, 274–287 (2013).
- <sup>12</sup>F. Bingöl, J. Mann, and G. C. Larsen, "Light detection and ranging measurements of wake dynamic. Part I: One-dimensional scanning," *Wind Energy* **13**, 51–61 (2010).
- <sup>13</sup>J.-J. Trujillo, F. Bingöl, G. C. Larsen, J. Mann, and M. Kühn, "Light detection and ranging measurements of wake dynamics. Part II: Two-dimensional scanning," *Wind Energy* **14**, 61–75 (2011).
- <sup>14</sup>S. Schreck, "The NREL full-scale wind tunnel experiment," *Wind Energy* **5**, 77–84 (2002).
- <sup>15</sup>H. Snel, J. Schepers, and B. Montgomerie, "The MEXICO project (model experiments in controlled conditions): the database and first results of data processing and interpretation," *J. Phys.: Conf. Ser.* **75**, 012014 (2007).
- <sup>16</sup>M. Khan, Y. Odemark, and J. H. Fransson, "Effects of inflow conditions on wind turbine performance and near wake structure," *Open J. Fluid Dyn.* **7**, 105 (2017).
- <sup>17</sup>H. Hangan, "The wind engineering energy and environment (WindEEE) dome at Western University, Canada," *Wind Eng. JAWE* **39**, 350–351 (2014).
- <sup>18</sup>A. Hassanzadeh, A. Kirby, R. Roy, D. Mavriplis, M. Stoellinger, and J. Naughton, "Design and numerical validation of a small scale wind turbine blade for scaled wake testing," (unpublished) (2021).
- <sup>19</sup>D. M. Somers, "Design and experimental results for the S814 airfoil," Technical Report No. NREL/SR-500-36345 (National Renewable Energy Laboratory, Golden, CO, 1997).
- <sup>20</sup>D. M. Somers, "Design and experimental results for the S825 airfoil," Technical Report No. NREL/SR-500-36346 (National Renewable Energy Laboratory, Golden, CO, 2005).
- <sup>21</sup>A. Hassanzadeh, T. Harms, and J. W. Naughton, "Static and dynamic aerodynamic performance parameters for S814 and S825 airfoils at moderate Reynolds number," AIAA Paper No. AIAA 2019-0802, 2019.
- <sup>22</sup>A. Hassanzadeh Hassanabad, "Design, instrumentation development, and testing of a wind turbine blade for sub-scale wake testing," Ph.D. dissertation (University of Wyoming, 2019).
- <sup>23</sup>TFILtd, see <https://www.turbulentflow.com.au/products/cobraprobe/cobraprobe.php> for "Cobra Probe, Turbulent Flow Instrumentation Pty Ltd (2011)" (last accessed May 9, 2021).
- <sup>24</sup>A. Hassanzadeh, J. W. Naughton, J. LoTufo, and H. Hangan, "Aerodynamic load distribution and wake measurements on a sub-scale wind turbine," *J. Phys.: Conf. Ser.* **1452**, 012059 (2020).
- <sup>25</sup>J. Naughton, J. Strike, M. Hind, A. Magstadt, and A. Babbitt, "Measurements of dynamic stall on the DU wind turbine airfoil series," in AHS Forum (2013), Vol. 69.
- <sup>26</sup>J. Strike, M. Hind, M. Saini, J. Naughton, M. Wilson, and S. Whitmore, "Unsteady surface pressure reconstruction on an oscillating airfoil using the Wiener deconvolution method," AIAA Paper No. AIAA 2010-4799, 2010.
- <sup>27</sup>M. Hind, P. Nikoueeyan, and J. Naughton, "Quantification of uncertainty in the correction of remotely measured unsteady pressure signals on pitching airfoils," AIAA Paper No. AIAA 2017-3733, 2017.
- <sup>28</sup>P. Nikoueeyan, M. Hind, J. Strike, M. Singh, J. Naughton, S. Keeter, and M. Dahland, "Characterization of unsteady pressures on a blunt trailing edge using a direct-mount pressure scanner," AIAA Paper No. AIAA 2019-1827, 2019.
- <sup>29</sup>P. Medina, M. Singh, J. Johansen, A. R. Jove, E. Machefaux, L. Fingersh, and S. Schreck, "Aerodynamic and performance measurements on a Swt-2.3-101 wind turbine," Technical Report No. NREL/CP-5000-51649 (National Renewable Energy Laboratory, Golden, CO, 2011).
- <sup>30</sup>R. J. Adrian and J. Westerweel, *Particle Image Velocimetry* (Cambridge University Press, 2011).
- <sup>31</sup>R. Kilpatrick, H. Hangan, K. Siddiqui, D. Parvu, J. Lange, J. Mann, and J. Berg, "Effect of Reynolds number and inflow parameters on mean and turbulent flow over complex topography," *Wind Energy Sci.* **1**, 237–254 (2016).
- <sup>32</sup>A. Fouras and J. Soria, "Accuracy of out-of-plane vorticity measurements derived from in-plane velocity field data," *Exp. Fluids* **25**, 409–430 (1998).
- <sup>33</sup>J.-M. Foucaut, J. Carlier, and M. Stanislas, "Piv optimization for the study of turbulent flow using spectral analysis," *Meas. Sci. Technol.* **15**, 1046 (2004).
- <sup>34</sup>L. P. Chamorro and F. Porté-Agel, "A wind-tunnel investigation of wind-turbine wakes: Boundary-layer turbulence effects," *Boundary-Layer Meteorol.* **132**, 129–149 (2009).
- <sup>35</sup>W. Tian, A. Ozbay, and H. Hu, "Effects of incoming surface wind conditions on the wake characteristics and dynamic wind loads acting on a wind turbine model," *Phys. Fluids* **26**, 125108 (2014).